CHEMISTRY OF MATERIALS

pubs.acs.org/cm

Article

Elucidating Structural Transformations in $Li_xV_2O_5$ Electrochromic Thin Films by Multimodal Spectroscopies

Angelique Jarry,* Mitchell Walker, Stefan Theodoru, Leonard J. Brillson, and Gary W. Rubloff

Cite This: *Chem. Mater.* 2020, 32, 7226−7236

Read Online

ACCESS | Metrics & More | Article Recommendations | Supporting Information

ABSTRACT: Vanadium oxides are widely seen as strong candidates for next-generation energy-saving electrochemical devices, ranging from their use as cathode materials in inherently safe high energy all-solid-state batteries to smart windows that employ their wide color range of electrochromic response. However, critical questions about these materials remain largely unanswered: interfacial reactions and the evolution of the electrode material as delithiation takes place. Distinguishing between topotactic (i.e., reversible) intercalation, conversion, and alloying reactions in ion tunable vanadium oxide devices, in operando, at a resolution that matches the size of structural building units, is a particularly challenging task. In this work, we investigated the effects of lithiation on the structural and optical characteristics of a model thin film system - $Li_xV_2O_5$ - as a function of depth, using several highly sensitive and nondestructive spectroscopic methods with different depth sensitivities. We exploit (1) $Li_xV_2O_5$ electrochromic properties to utilize in operando optical response, (2) depth-resolved cathodoluminescence spectroscopy (DRCLS), and (3) Raman spectroscopy to monitor the changes in $Li_xV_2O_5$ electronic structure from the surface to the bulk of the thin film with nanoscale resolution. We find that the degradation of electrochemical performance with deep discharge of $Li_xV_2O_5$ is associated with drastic band structure changes that accompany octahedral distortion, rather than with a chemical conversion reaction. Elongation along the *c* axis and charge redistribution induced by varying levels of V(3d)−O(2p) hybridization in the presence of the Li considerably affect the electronic band structure. The coexistence of multiple metastable phases, strong electron correlation, and deviation from an ideal cubic symmetry results in lower structural reversibility with a higher bandgap. Beyond these specific inferences, these results suggest that these optical techniques—Raman, optical absorption/reflection, and cathodoluminescence—can be a powerful combination to reveal electrochemical behavior of ion-tunable transition metal oxides materials and associated reaction mechanisms.

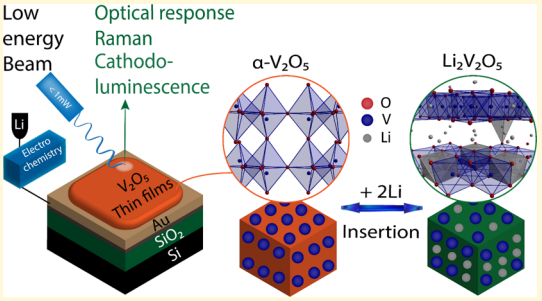

INTRODUCTION

Further development of high-energy batteries is hampered by the current lack of understanding and control of interfacial processes and associated phases formed upon cycling as well as the low cathode capacity.[1,2] The latter can be addressed with layered oxide cathode materials, allowing the intercalation of multiple lithium atoms per formula unit of cathode material, a strategy that has attracted considerable attention from the battery community in recent years.[3−9]

V_2O_5 is of particular interest due to the large interlayer spacing of its metastable varieties that allows deintercalation of various cations ($M_xV_2O_5$ withM = Li, Na, and Mg and 0 < X < 3).[3,10,11] V_2O_5 can intercalate up to three lithium per V_2O_5 formula unit, approaching a theoretical capacity of 440 mAh/g.[12] This exceeds the capacity of the leading transition metal based cathode candidates for high energy Li-cells, e.g., Ni-rich NMCs (~200 mAh/g)[4,13] or Li-excess disordered rock salt structures (Li_xDRS).[4−8]

However, this cation deinsertion can lead to structural distortion associated with the coexistence of multiple metastable phases and variations in the electronic band structure that impede cathode performance.[14−16] In fact, while the intercalation of lithium into the V_2O_5 host lattice is mostly topotactic, partial conversion reactions may occur, if certain criteria are met, leading to capacity fading.

Investigations using multiprobe approaches have confirmed that surface composition, defects, host structure, and morphology of the cathode itself have a substantial impact on these degradation mechanisms.[15−18] However, the exact role of the surface chemistry and nature of the structural rearrangement (i.e., insertion versus conversion) on the performance of electrochemical systems is still subject to debate. These uncertainties are due to the intricate nature of the mechanisms in play, together with the inherent limitations of the characterization methods on which the knowledge relies.

Received: April 7, 2020
Revised: August 15, 2020
Published: August 18, 2020

Downloaded via UNIV OF MARYLAND COLG PARK on September 21, 2020 at 21:06:22 (UTC).
See https://pubs.acs.org/sharingguidelines for options on how to legitimately share published articles.

ACS Publications

© 2020 American Chemical Society

https://dx.doi.org/10.1021/acs.chemmater.0c01478
Chem. Mater. 2020, 32, 7226−7236

Although they provide extremely valuable information, most of the experimental investigations have been carried out using high energy source methods such as electron energy loss spectroscopy (EELS),[16,17,19] XANES,[20] TEM,[13] SAED,[2] SEM,[17,21] or XRD[3,22,23] that can easily induce beam damage to a battery materials system.[24] Therefore, to understand how to overcome the barriers related to the implementation of high energy-power SSBs, there is substantial benefit to starting with pure, well-defined models and systems such as cathode thin films and performing advanced diagnostic studies using innovative nondestructive tools.

Vanadium oxide thin films can be grown easily by sputtering or ALD methods.[25−28] V_2O_5 is an electrochromic material, with a bandgap in the visible spectrum, i.e., ∼2 eV, which translates into a bright orange color.[29,30] Any variation in lithium content will impact the vanadium oxidation state and hybridization of the vanadium 3d − O 2p orbitals, which is notably evident in the optical properties as a color change.[28−32] Consequently, the electrochromic effect of $Li_xV_2O_5$ systems offers a direct and unique insight into battery operation, including the structural evolution of $Li_xV_2O_5$, especially in combination with other nondestructive spectroscopic methods such as Raman spectroscopy (RS) and depth-resolved cathodoluminescence spectroscopy (DRCLS).

In this work, we investigate the impact of lithiation on the nature of the structural rearrangement in $Li_xV_2O_5$ thin films and associated long-term electrochemical performance. Changes in the crystallinity, local atomic structure, and associated electronic properties were probed with RS, optical imaging, and DRCLS. DRCLS employs a rather low energy electron beam in the range 0.5−3 keV to minimize the risk of beam damage. The correlation between the lithium content, cycling number, structural stability, electronic properties, and electrochemical performance are discussed.

EXPERIMENTAL SECTION

V_2O_5 Thin Film Preparation. V_2O_5 thin films of ∼500 nm were produced by atomic layer deposition (ALD) on gold-coated silicon substrates of 1 cm × 1 cm. The silicon substrate was prepared as follows: the wafer was first wet etched in HF to remove any surface impurities. Then a 500 nm SiO_2 passivation layer was thermally grown in an Oxford Plasmalab system 100. A 20 nm chrome adhesion layer followed by a 200 nm gold current collector layer was deposited by sputtering in an AJA ATC Orion 8 sputtering system. The 3-in. diameter gold-coated wafer was diced into 1 cm × 1 cm squares. The V_2O_5 ALD layer was grown onto the square substrates using a stainless steel shadow mask. The ALD V_2O_5 process was performed at 170 °C in a BENEQ TFS 500 reactor[26] using vanadium tri-isopropoxide (VTOP) as the vanadium precursor and ozone as the oxidant. The V_2O_5 film thickness was measured ex-situ using a profilometer.

Chemical Lithiation. In situ optical spectroscopy measurements were performed using a three-electrode spectro-electrochemical cell for lithiation. The spectro-electrochemical cell was filled with PC 1 M $LiClO_4$ electrolyte and cycled galvanostatically between 3.4 and 2.2 or 2.8 V at a scan rate of ∼C/2 corresponding to a current of 2 μA using a Biologic VMP3 potentiostat. A dwell time of 5 h at the high or low cutoff voltage enabled the system to reach equilibrium. Images were recorded every 10 min using a Dino-Lite camera. Every experiment was repeated at least 3 times to ensure the reproducibility of the results. The samples were removed from the cell at the desired voltage/state of charge, i.e., 3.4, 2.8, or 2.2 V, and washed extensively in pure PC to remove any remaining solid electrolyte interphase/Li salt and dried in vacuum for at least 20 min in a glovebox antechamber prior to ex-situ measurements.

$Li_xV_2O_5$ Sample Characterization. Atomic force microscopy (NT-MDT, NTEGRA Spectra) was used to determine the surface roughness of the samples before and after lithiation (Supporting Information, Figure S1). Raman spectroscopy measurements were recorded in the backscattering configuration with a confocal "LabRam" microscope system (Horiba Jobin Yvon U.S.A.) equipped with a 633 nm laser source (laser power adjusted to ≤1 mW, ∼2 μm beam diameter). An airtight cell compatible with the Raman system and a long working distance microscope objective with 50× magnification (Olympus America Inc.) were used. Exposure time and the number of repetitions (X) were adapted to acquire high-quality spectra. Three Raman spectra with the same exposure time were collected and compared in the following sequence: 1 repetition, X repetitions, 1 repetition, to ensure the absence of beam damage that could induce undesired phase transitions.[34]

DRCLS spectra were collected using a custom-made ultrahigh vacuum chamber, glancing incidence electron gun and optics equipped with a CCD detector and an electron beam focal resolution of 0.3 mm. The incident beam energy was varied from 0.5 to 3 keV to collect information from various depths. Monte Carlo simulations were used to determine the theoretical electron−hole pair creation rate versus depth, e.g., the excitation depth of the beam within the V_2O_5 thin films. (Table 1). Monte Carlo simulations were carried out with CASINO (Monte Carlo simulation of electron trajectory in solids) software.[33,34]

Table 1. Theoretical Depth Penetration Values in V_2O_5 Calculated by Monte Carlo Simulations with CASINO as a Function of Depth-Resolved Cathodoluminescence (DRCLS) Incident Photon Energy

DRCLS beam energy(KeV)	0.5	1	1.5	2	2.5	3
depth penetration in V_2O_5 (nm)	8	20	37	57	80	107

RESULTS

Electrochromic Properties of $Li_xV_2O_5$. Potential uses for $Li_xV_2O_5$ are multifold. Due to its electrochromic properties, its applications include not only batteries but also smart windows, displays, and rear-view mirrors.[30] Intercalation of small ions such as lithium into a layered α-V_2O_5 structure is accompanied by reversible redox reactions involving different vanadium oxidation states with significant changes in the density of states. With a bandgap in the visible spectrum, the optical properties and associated colors are correlated to the $Li_xV_2O_5$ lithiation level. The lithium diffusion rate and the number of intercalation sites control the switching frequency and color contrast, respectively. Any significant cathode structural degradation or state of charge inhomogeneity will be reflected in the optical properties.[28−32] Therefore, the optical response of the system during electrochemical cycling can be used as a diagnostic tool to probe the lithiation level and associated phase present.

Extensive details regarding the expected structural evolution of $Li_xV_2O_5$ as a function of the lithiation level as dictated by the electrochemistry are given in SI Figure S2. As displayed in Figure 1, the electrochemistry of $Li_xV_2O_5$ was performed in a custom-made 3-electrode cell configuration allowing the simultaneous collection of the electrochemical and optical responses. Figure 1 shows the first galvanostatic charge and discharge cycle of the $Li_xV_2O_5$ ($0 < x < 2$) thin-film between 3.4 and 2.2 V at a ∼C/10 rate, e.g., 10 h for a charge, which translates into applying a ±2 μA current. From high to low voltage, the expected phase transformations ($\alpha \rightarrow \varepsilon \rightarrow \delta \rightarrow \gamma$) along the three plateaus at 3.4, 3.2, and 2.3 V (vs Li/Li^+) are

https://dx.doi.org/10.1021/acs.chemmater.0c01478
Chem. Mater. 2020, 32, 7226−7236

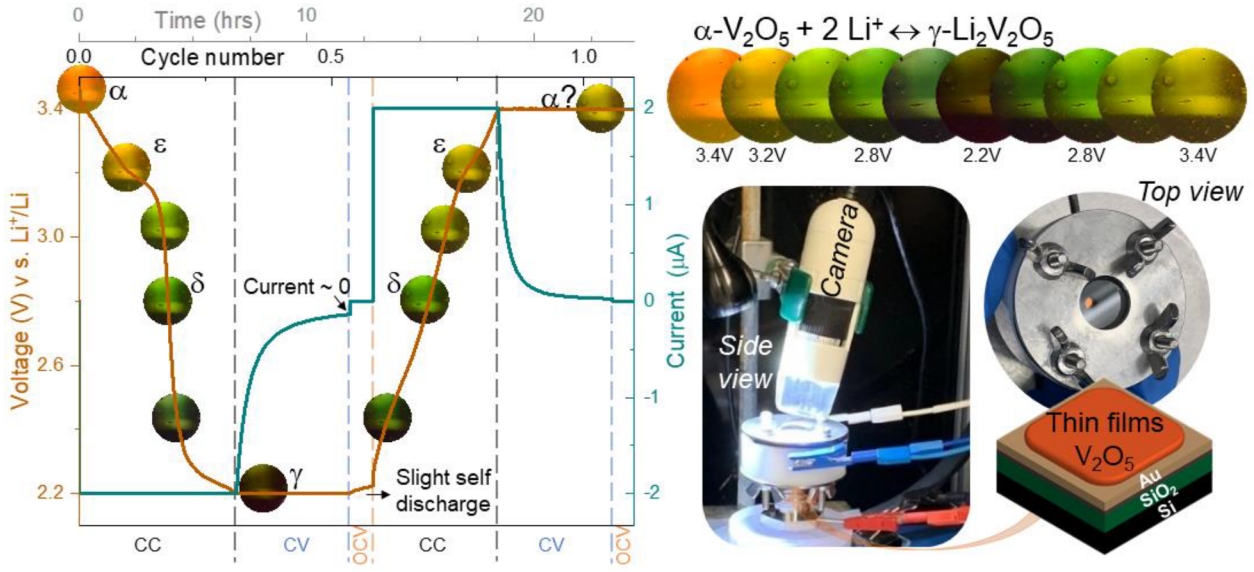

Figure 1. Electrochemical and optical response of $Li_xV_2O_5$ ($0 < x < 2$) as a function of voltage. V_2O_5 thin films were cycled galvanostatically from 3.4 to 2.2 V vs Li^+ (counter and reference) with a current of 2 μA (corresponding to ~C/10: 10 h to lithiate) in 1 M $LiClO_4$ in PC in a custom electrochemical cell (CC region). Voltage was maintained 5 h at high and low cut off voltage to allow the system to reach equilibrium (CV region). After the dwell period and before the charge or discharge the voltage variation was recorded for 1 h at open circuit voltage (OCV region). The custom electrochemical cell is designed with a 5 mm diameter opening that exposes the V_2O_5 to the electrolyte and corresponds to the size of the optical images that were recorded every 10 min.

observed. At the low cut off voltage of 2.2 V where γ-$Li_2V_2O_5$ is obtained, an additional dwell time of 5 h is applied to ensure the formation of a single homogeneous phase. At the end of the dwell time, the current value is nearly 0 μA, confirming that the system has reached equilibrium. The voltage is then recorded during a 1 h relaxation period, at open-circuit voltage, to assess the potential self-discharge phenomenon. This sudden switch-off current is an indirect measurement of the polarization effect and associated internal resistance of the system.[35] As inferred from the current profile, the slight increase of voltage over this period (20 mV/h) is consistent with a stabilization of the phase. A similar protocol is employed for the discharge, where the profile appears quasisymmetric to the charge profile, with the phase transformations corresponding to the deintercalation process ($\gamma \rightarrow \delta \rightarrow \varepsilon \rightarrow \alpha$).

During the electrochemical experiments, an optical camera was used to record an image of the thin film through the quartz windows and transparent liquid electrolytes every 10 min (Figure 1). In accordance with the electrochromic behavior of $Li_xV_2O_5$, a gradual change in the optical response is observed during the insertion of two lithium per unit cell within the structure. In agreement with prior work,[29,30] the color varies with cell potential and associated phase transformations, from the orange oxidized state (3.4 V: α-V_2O_5), to a yellow gold (3.2 V: ε-$Li_xV_2O_5$), to light green (2.8 V: δ-LiV_2O_5), and finally to a darker green in the reduced state (2.2 V: γ-$Li_2V_2O_5$). During the lithium deintercalation process, symmetric coloration is observed with a film turning back from green to yellow gold. However, at the highest cutoff voltage (3.4 V) and even after the dwell time of 5 h, the films do not exhibit the orange color characteristics of the pristine α-V_2O_5. This color discrepancy is the first indication that the intercalation of two lithium can result in irreversible phase transformation. The apparent inhomogeneity in the color of the images is related to the setup used in this experiment. For sufficient lighting, the camera needed to be placed at an angle, which created a shadowing effect due to the PEHD body (bottom) and a reflection effect on the sample (lower end).

Electrochemical Performance of $Li_xV_2O_5$. As shown in Figure 2, to assess the reversible nature of the phase transformations and establish the correlation with the electrochemical performance and optical response, the galvanostatic charge−discharge cycling of $Li_xV_2O_5$ described above was repeated multiple times. Two voltage windows were used, i.e., 3.4−2.2 V and 3.4−2.8 V for a $0 < x < 2$ and $0 < x < 1$ composition range, respectively.[36] The applied ±2 μA current was kept constant to maintain a similar lithiation insertion rate. A photo of the thin film was taken in operando every 10 min for the entire duration of the experiments.

Battery performance metrics are given in Table S1 of the Supporting Information. The galvanostatic curves show the expected insertion and deinsertion steps corresponding to $\alpha \leftrightarrow \varepsilon \leftrightarrow \delta \leftrightarrow \gamma$ transitions for the 3.4−2.2 V voltage range. Charge consumed corresponds to a specific capacity delivered of 262 mAh/g with the accommodation of two lithium per unit of vanadium oxide (Figure 2a−d). It should be noted that the apparent added capacity during the dwell time is most likely partially related to chemical diffusion of lithium in the V_2O_5 electrodes. In the electrochemical cell, the effective working area, i.e.,V_2O_5 surface, exposed to the liquid electrolyte is ~20 mm^2, while the V_2O_5 total sample area is 64 mm^2. A lithium chemical gradient diffusion may take place over time. Accordingly, to avoid any misinterpretation, the delivered capacity is calculated from the value obtained at the beginning of the dwell step. Over the 6 cycles, limited capacity fading is observed.

However, at low voltage (2.2 V), the polarization effect becomes stronger as the cycle number increases, going from 20 to 80 mV/h (Table S1). The same applies to the internal resistance, i.e., resistance calculated from Ohm's law with the voltage variation between before and 30s after the current switch-off. The resistance increases from 1750 Ω to 5000 Ω

https://dx.doi.org/10.1021/acs.chemmater.0c01478
Chem. Mater. 2020, 32, 7226−7236

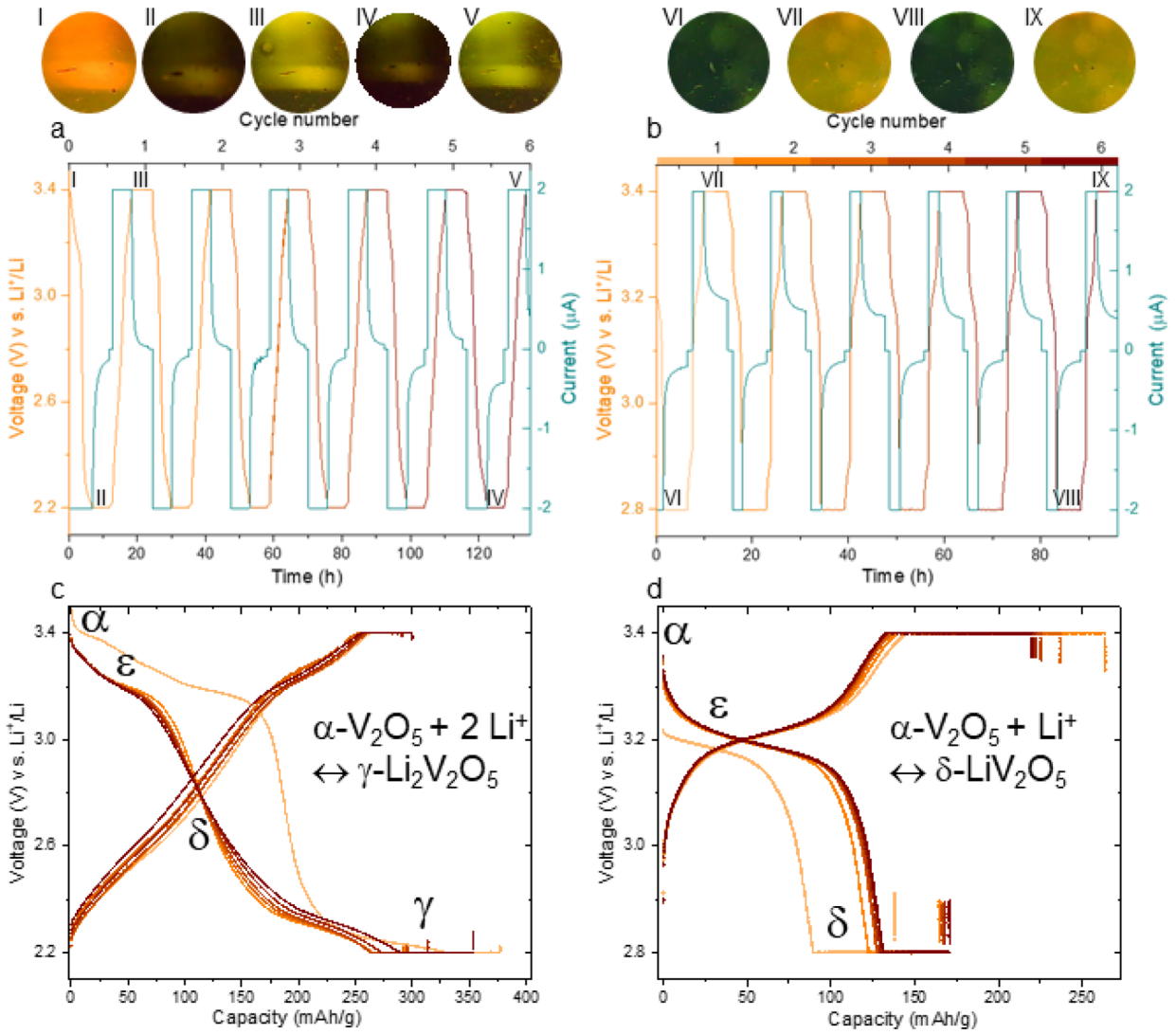

Figure 2. Electrochemical and optical response of $Li_xV_2O_5$ ($0 < x < 2$) as a function of voltage range and cycling number. V_2O_5 thin films were cycled galvanostatically 6 times from 3.4 to 2.2 V (a and c) or 2.8 V (b and d) vs Li+ (counter and reference) with a current of 2 μA in 1 M $LiClO_4$ in PC in a custom electrochemical cell. Voltage was maintained for 5 h at the high and low cut off voltage to allow the system to reach equilibrium. The custom electrochemical cell is designed with a 5 mm diameter opening that exposes the V_2O_5 to the electrolyte and corresponds to the size of the optical images (a and b). Roman numerals (a and b) refer to specific states that are discussed in detail in this study. Electrochemical response was used to extract and follow the evolution of the capacity delivered together with the corresponding theoretical phase transition (c and d).

after 6 cycles. As expected with a ~500 nm thin film and considering the 30 s waiting time, the resistance value is high but nonetheless consistent with the values reported in the literature.[37] One should notice that at the high cut off voltage (3.4 V), the polarization and internal resistance values are lower, going from 3 to 26 mV/h and from 350 to 2175 Ω after 6 cycles, respectively. This increase of internal resistance suggests a degradation mechanism involving the creation of multiple Li^+ conduction pathways. Considering the good capacity retention and limited polarization, this raises the possibility of a gradual formation of a minor secondary phase forming inclusions that will mostly reduce the lithium diffusion rate without significantly affecting the amount of lithium inserted overall. The sluggish diffusion at the boundary between the phases would result in a higher interfacial resistance, i.e., the increase of internal resistance observed.

This proposed degradation mechanism is supported by the color variation observed while cycling. During charging, the materials exhibit a continuous color change, going from orange (Figure 2a I), to yellow, to dark green (Figure 2a II). However, at 3.4 V, the sample is yellow rather than orange (Figure 2a III). Moreover, as cycling goes on, the color appears closer to light green (Figure 2a V). This gradual color deviation implies that the amount of lithium remaining in the structure at high voltage is increasing. The global homogeneity of the color indicates that, if multiple phases coexist, they must blend at the macroscale.

Figure 2c,d displays the galvanostatic curves between 3.4 and 2.8 V. 2.8 V is below the $\varepsilon \leftrightarrow \delta$ but above $\delta \leftrightarrow \gamma$ phase transition plateau. At this voltage, one would expect to retain the δ-$Li_xV_2O_5$ phase with $x = 1$. The delivered capacity value was used as a means to confirm the lithium content. The value was determined to be 145 mAh/g, which is about two times smaller than the value calculated with the 3.4−2.2 V voltage range, confirming the intercalation of one lithium. Over the 6 cycles, the capacity retention is good, and the charge−discharge profile is symmetric. These results suggest high reversibility of the lithium intercalation process. The cycling

https://dx.doi.org/10.1021/acs.chemmater.0c01478
Chem. Mater. 2020, 32, 7226−7236

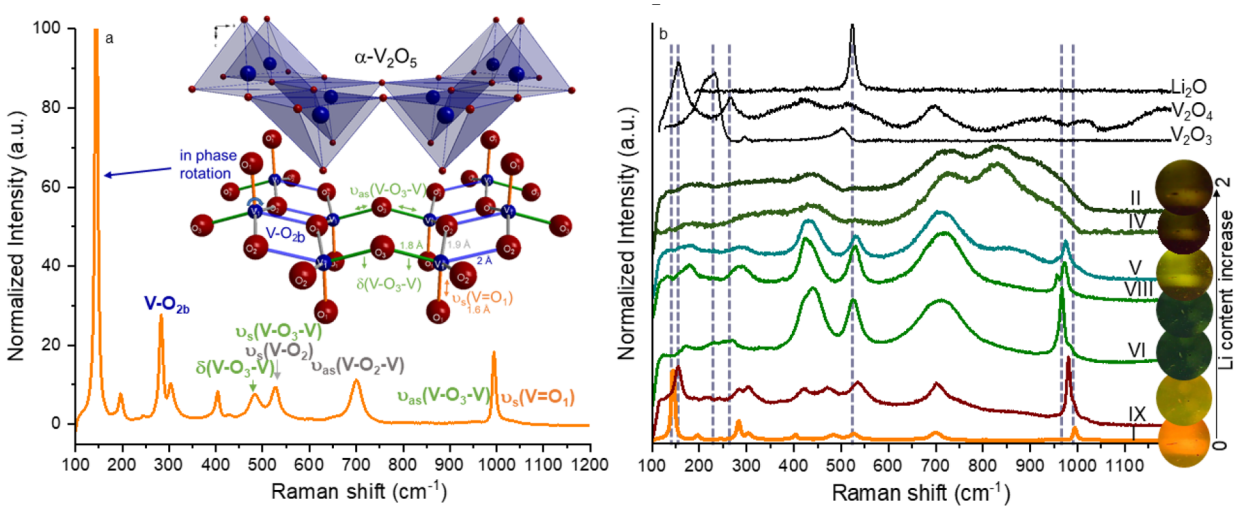

Figure 3. (a) Crystallographic representation of α-V_2O_5 with the corresponding Raman spectra and vibrations assignments. (b) Raman spectra of $Li_xV_2O_5$ as a function of lithiation level x and cycling number indicated with Roman numerals and images corresponding to specific states in accordance with Figure 2. Raman spectra of reference powders Li_2O and V_2O_4 were added for a direct comparison.

number's impact on the polarization and internal resistance values has been investigated. As displayed in Figure 2c and d and in Table S1, the values are significantly higher than for the 3.4−2.2 V, and especially for the 2.8 V low cutoff voltage. This peculiar increase is most likely a consequence of the metastable state of δ-$Li_xV_2O_5$ which can easily gain or lose lithium, ranging over 6 cycles from, at high voltage, 80 to 45 mV/h and 5500 to 4000 Ω and at low voltage, 111 to 97 mV/h and 12000 to 8950 Ω. Interestingly, the values are lower at high voltage but decrease with the cycling number, indicating that the system is stabilizing over time rather than degrading.

The impact of the lithium deintercalation process on the optical response was also considered. A constant color change correlated to the voltage is observed, going from yellow at high voltage (Figure 2c VII and IX) to a forest green at low voltage (Figure 2c VI and VIII). Notably, these two colors coincided with the shade initially observed at 3.4 and 2.8 V for the galvanostatic cycling in the 3.4−2.2 V range. The major difference remains in the consistency of the overall color at high voltage.

Local Structure of $Li_xV_2O_5$ by Raman Characterization. By investigating the correlation between Raman spectroscopy and the optical response, we gain additional insight into vanadium oxidation states and local chemical environments as a function of lithiation level and number of cycles. Raman spectroscopy has been extensively used to probe the effect of lithium intercalation on the local structure of battery materials.[34,22] As a matter of fact, Raman peaks assignment for α, δ, ε, and γ-LiV_2O_5 (powder or thin films) has been discussed in great detail elsewhere.[23,27,38−41] Raman frequencies are known to be extremely sensitive to variations of vanadium oxide oxidation state, vanadium−oxygen bond distance, as well as structural distortion at the atomic scale. With a typical spatial resolution of 1 μm, Raman mapping has been successfully used to investigate quantitative phase transitions, formation of microphases, inclusions, and related degradation mechanisms resulting in nonuniform transport kinetics across transition metal oxide materials.[42,43] Hence, confocal Raman microspectrometry, with a laser power maintained <1 mV to prevent any risk of beam damage, is ideal for examining the nature of the phases present in our $Li_xV_2O_5$ thin films.

Raman spectra of selected $Li_xV_2O_5$ thin films are presented in Figure 3, together with the corresponding optical response. The samples were removed from the electrochemical cell at a specific cutoff voltage and prepared as described in the Experimental Section. Every experiment was repeated at least 3 times on different samples and different locations in the airtight cell. The 7 types of samples were chosen per the electrochemical and optical response results discussed above, i.e., I, II, IV, V, VI, VIII, and IX, at the most significant cutoff voltage and cycling number (see Figure 2). First, it should be noted that for all the samples, the same spectra were obtained independently of the location.

The typical Raman spectra and crystal structure of α-V_2O_5 with the corresponding Raman peak assignment are presented in Figure 3a. As described in Figure S1, α-V_2O_5 adopts an orthorhombic space group *Pmmn*. The structure consists of 4 nonequivalent atomic positions (V, O_1, O_2, and O_3), which give rise to four distinctive bond lengths and types: a strong and short vanadyl V═O1 apical bonds (d = 1.6 Å orange), a bridge bond V−O_3 (d = 1.6 Å green), two equivalent intraladder V−O_2 bonds (d = 1.9 Å gray), and finally an interchain V−O_2 bond (d = 2 Å blue). Together they form the compressed VO_5 pyramid basic motif of the crystal host lattice.

While there are 21 theoretical Raman-active modes, only 9 peaks can be easily distinguished.[34] The main reasons for this are the close frequencies and the low scattering intensity of some modes. From the vibrational assignments, it is clear that all modes above 480 cm^{-1} are bond-stretching vibrations (symmetric or asymmetric) and that the stronger and longer the V−O bonds are, the higher the Raman shift. Out of plane V = O_1 symmetric bond-stretching is at particularly high frequency (995 cm^{-1}) due to the double bond. It should be emphasized that vibrations related to O_3 displacements are not seen as a consequence of a cancellation effect in the highly symmetric system. The 700 and 525 cm^{-1} vibrations involve O_2 displacements. Starting from 480 cm^{-1} and below, Raman shifts can be attributed to bending modes with considerable coupling. Bending deformations related to the V−O_3 bridge are seen at 480 and 400 cm^{-1}. Finally, the most intense peak at

https://dx.doi.org/10.1021/acs.chemmater.0c01478
Chem. Mater. 2020, 32, 7226−7236

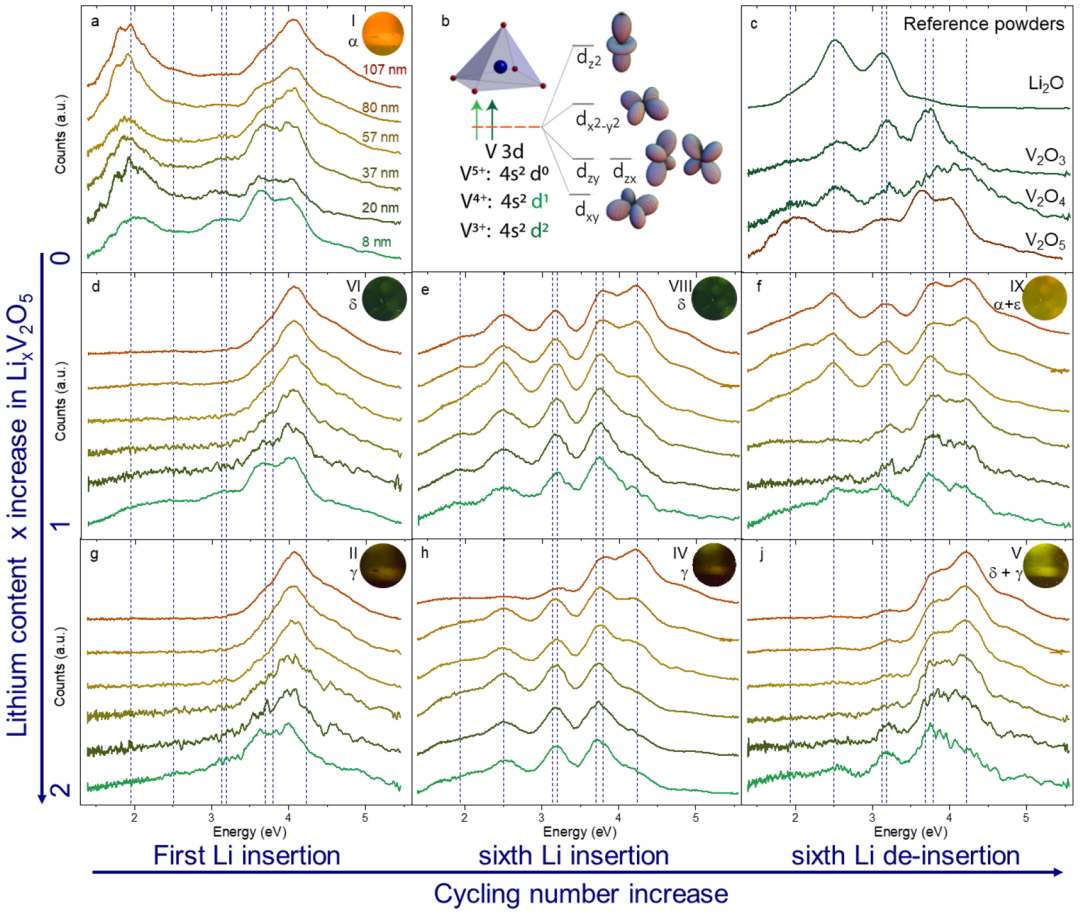

Figure 4. (a and d–j) DRCLS spectra of $Li_xV_2O_5$ thin films as a function of: (1) incident beam energy-penetration depth (0.5 keV (8 nm—bright green), 1 keV (20 nm dark green), 1.5 keV (37 nm yellow-green), 2 keV (57 nm yellow), 2.5 keV (80 nm yellow-orange), and 3 keV (107 nm-orange)); (2) lithiation level x and cycling number with Roman numerals, Greek letters, and images corresponding to specific states/metastable phases per Figure 2 and 3. (b) V 3d orbital state levels in the theoretical band structure of α-V_2O_5. (c) DRCL spectra of reference powders.

143 cm^{-1} involves in-phase rotation and can be leveraged as a pointer to the long-range ordering of the V—O framework in the plane.

Figure 3b compares the Raman spectra of the pristine α-V_2O_5 (I) with cycled samples (II, IV, V, VI, VIII, and IX) and reference powders (Li_2O, V_2O_4, and V_2O_3). All spectra were normalized to 100 and offset in the y-axis to facilitate the interpretation. It should be stressed that the intensity of the peaks decreases drastically with lithium content. As a consequence, the spectra V, VII, and VIII ($Li_xV_2O_5$ with $x \approx 1$) and even more so II and IV ($Li_xV_2O_5$ with $x \approx 2$) exhibit lower signal-to-noise/background ratio. This intensity quenching is an indication of progressive amorphization of the sample, in agreement with the reduction of roughness observed by AFM as lithium content increases (Supporting Information, Figure S2).

As expected, lithium uptake, voltage range, and cycling number impact the Raman spectral signature. Samples VI, VIII and IX were cycled from 3.4 to 2.8 V but removed from the cell at different states of charge or cycling number (see Figure 2c). Lithium uptake within the V_2O_5 host lattice alters atom movements. The emergence of O_1—Li bonds together with an increase of the degree of disorder/puckering strongly affects the position and intensity of the Raman peaks at 995 and 143 cm^{-1}. Raman spectrum VI refers to a sample that has been through half a cycle up to 2.8 V. Hence δ-LiV_2O_5 is expected. Our Raman data is consistent with this assumption as it appears similar to Raman spectra of the δ-LiV_2O_5 thin film previously reported in the literature.[24,40] Notably, the peak at 143 cm^{-1} is extinct and we observed a shift from 995 to 967 cm^{-1}, consistent with a higher level of disorder and a V—O_1 bond elongation-weakening. The shoulder on the right of 967 cm^{-1}, at 982 cm^{-1}, signals the existence of multiple V—O_1 stretching modes. Interestingly, by comparison with the Raman spectrum VIII, which went through more cycling, the shoulder shifts down to 957 cm^{-1} while the central peak is at 972 cm^{-1}. These results are in perfect agreement with prior works24 and 40 which identify the coexistence of δ-LiV_2O_5 with either ε (982 cm^{-1}) or γ (957 cm^{-1}). IX corresponds to a cycle history where α-V_2O_5 should be attained. As suspected from the yellow color of the sample IX, compared to the pristine α-V_2O_5 orange (I), the peaks at 143 and 995 cm^{-1} never recover their original position and intensity. Moreover, additional Raman modes are observed in the IX spectra. A more precise examination reveals that the additional Raman modes match very well with a Li-poor ε-$Li_xV_2O_5$ Raman fingerprint reported in the literature.[24,34,23]

Samples II, IV, and V were cycled from 3.4 to 2.2 V (see Figure 2b). As a result of their electrochemical history, samples II and IV should be γ-$Li_2V_2O_5$ phase. Our spectra are consistent with reported vibrations of γ-$Li_2V_2O_5$ ALD thin films.[40,41] The pronounced intensity decrease and broadening

https://dx.doi.org/10.1021/acs.chemmater.0c01478
Chem. Mater. 2020, 32, 7226–7236

of all of the peaks is striking. The $V-O_1$ and 143 cm^{-1} signature peaks disappear as a shoulder of a peak at 930 cm^{-1} and two new broad peaks appear at 830 and 730 cm^{-1}. The high-frequency shoulder intensity diminishes with cycling numbers. The most plausible explanation for these behaviors is a high degree of disorder within the film and a drastic weakening of the $V-O_1$ bond at deep charge.

In principle, sample V should be an α-V_2O_5 phase. Consistent with the green color, the Raman spectra revealed a signature corresponding to a δ-LiV_2O_5 phase which is also a close match with Raman spectrum VIII. The existence of degradation product inclusions was also suspected by a comparison between the Raman spectra of our samples (II, IV, V, VI, VIII, and IX) and the reference powders (Li_2O, V_2O_4, and V_2O_3). As seen in Figure 2b, the main characteristic peaks of V_2O_4 (155 and 267 cm^{-1}) and V_2O_3 (223, 300, and 500 cm^{-1}) do not overlap with our samples' Raman signal, which demonstrated that they are either not present or in quantity below the Raman detection limits. The same applies to the only Li_2O Raman frequency signature that has some overlapping with α, ε, and δ-$Li_xV_2O_5$ excitations but not with the γ-$Li_2V_2O_5$ spectra.

Electronic Structure of $Li_xV_2O_5$ by Depth-Resolved Cathodoluminescence Spectrocopy (DRCLS). Cathodoluminescence (CL) has been widely used for decades, largely to characterize and identify defects in geological materials, and it has since evolved significantly for use with semiconductors.[44,45] Tremendous innovations in a variety of fields such as photonics, microscopy, and detectors have directly benefited CL capabilities.[44,45] The spatial and depth resolution now extends down to the nanoscale with a sensitivity to alterations in electronic structure that are orders of magnitude higher than other methods, while using a relatively low incident beam energy of only a few keV.[44,45] Despite these advantages, the use of CL to characterize electronic features of battery cathode materials has been unexplored.[46] However, as battery performance relies heavily on local lattice distortion as well as movements of defects at the interfaces under bias, DRCLS offers an excellent opportunity to gain detailed insight into battery operation.

DRCLS spectra of selected $Li_xV_2O_5$ thin films and their optical responses are gathered in Figure 4. For a direct comparison with the Raman spectra, the CL response of the same seven types of samples (I, II, IV, V, VI, VIII, and IX) were collected (see Figures 2 and 3). The incident beam energies were chosen according to Table 1 to probe optical transition energies from the free surface to the bulk of the films. To facilitate the comparison of spectral features and hence the discussion, all spectral intensities were normalized to unity and offset in y in an order corresponding to the increase of beam energy-penetration depth used. An illustration is given in Figure 4a where α-V_2O_5 spectra were collected with a 0.5 keV (8 nm−dark green), 1 keV (20 nm green), 1.5 keV (37 nm green), 2 keV (57 nm yellow), 2.5 keV (80 nm yellow-orange), and 3 keV (107 nm-orange) incident beam energy.

Cathodoluminescence spectra are produced by the generation and recombination of electron−hole pairs. A multitude of transitions between unoccupied conduction band states and the valence band edge are excited simultaneously. Hence, a cathodoluminescence spectrum can be seen as an experimental measure of the partial densities of states where any changes are easily detected. As discussed in the sections above, α-V_2O_5 exhibits a crystal structure where vanadium is in a compressed pyramidal environment of oxygen (Figures 3a and 4b). Hence, according to the crystal field theory, the V 3d states are, from the lowest to the highest level in the band structure, V 3d t_{2g}: d_{xy}, d_{zy}, d_{zx}, and V 3d e_g: $d_{x^2-y^2}$ and, d_{z^2} (Figure 4b) with 1−7 eV optical transitions to the valence band edge.[32] In our chamber configuration, a 1.3−5.3 eV working energy range is accessible due to the CCD detector limitations combined with the diffraction grating position. In this work, we are then efficiently probing the partial V 3d t_{2g} and O $_{2p}$ density of states (DOS). In our previous work,[47] we confirmed the excellent agreement between partial V 3d t_{2g} DOS of α-V_2O_5 calculated by DFT[32] and measured by CL. We highlighted that the 1.8−2 eV peaks is associated with the strong V $3d_{xy}$-O $2p_x/2p_y$ hybridization states and is very sensitive to any lattice distortion as well as reduction of vanadium associated with lithiation. As a matter of fact, the 1.8−2 eV peak vanished with substantial lithium uptake in $Li_xV_2O_5$ (Figure 4d−j).

Figure 4a,d,g allows a direct comparison of the CL spectra of $Li_xV_2O_5$ as a function of lithiation content for the first intercalation ($0 < x < 2$; 0.5 cycles). The feature corresponding to the V $3d_{xy}$-O $2p_x/2p_y$ hybridization at 1.8−2 eV vanished with lithium intercalation. Interestingly, while the second main feature remains a broad peak at 4.2 eV, the second minor feature shifts toward higher energy with penetration depth.

DRCLS was also used to investigate the effect of cycling number on the electronic structure. Figure 4d,e compare two samples prepared at 2.8 V, but after 0.5 and 6 cycles, respectively. The difference is remarkable and suggests severe changes in the vanadium environment. To facilitate the interpretation, CL spectra of lithium oxide reference powders that could possibly form during the battery operation[14,48] as inclusions, i.e., Li_2O, V_2O_4, and V_2O_3, were collected. Surprisingly, the ∼2.5, ∼3.1, and ∼3.75 eV features in Figure 4d,e are also visible in the V_2O_3 and Li_2O spectra. It should be emphasized that, as inferred by the increase in the signal-to-noise ratio, the intensity of Li_2O bands are 200 times stronger. Note that, in Figure 4d,e, the broad peak at 4 eV still remains and becomes more prominent as a function of depth. The exact same conclusion can be drawn with deeper lithium intercalation, with Figure 4g,h, which compare two samples at 2.2 V ($Li_xV_2O_5$ with $x \approx 2$), but after 0.5 and 6 cycles, respectively.

The reversibility aspect of these peculiar features corresponding to V_2O_3 rather than V_2O_5 was also assessed by DRCLS. To this purpose, Figure 4f,j display samples at 3.4 V after 6 cycles in the 3.4−2.8 and 3.4−2.2 V, respectively. By comparison between Figure 4e,f as well as h,j, one can explore the reversible nature of the change in the electronic structure after delithiation. In agreement with the Raman spectroscopy, electrochemical, and optical response discussed above, the samples do not recover their original states at high voltage. The distinct features in Figure 4f,j are intermediate between those of Figure 4d,e,g,h.

DISCUSSION: TOPOTACTIC VERSUS CONVERSION REACTIONS IN $LI_XV_2O_5$

Researchers have studied the V_2O_5 lithiation charge/discharge cycle for several decades. However, there is still an ongoing debate regarding the possible formation of Li_2O and V_2O_4 during the lithiation of α-V_2O_5, i.e., partial conversion reaction/lithium segregation, as an irreversible degradation mechanism, even with the insertion of only 2 lithium within the structure.[14,48] Studies based on bulk methods with, among

https://dx.doi.org/10.1021/acs.chemmater.0c01478
Chem. Mater. 2020, 32, 7226−7236

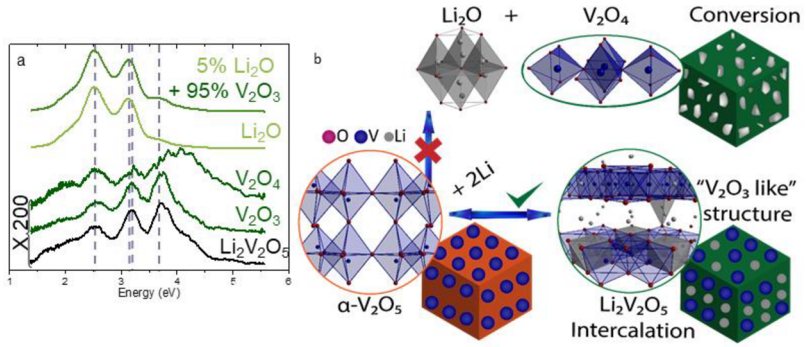

Figure 5. (a) CL spectra of reference powders V_2O_3,V_2O_4 and Li_2O as well as of sample IV (see Figures 2−4) corresponding to $Li_2V_2O_5$ cycled 5.5 times. The intensity of the V_2O_3,V_2O_4 and sample IV DRCL spectra have been increased by a factor of 200 compared to the Li_2O intensity. A linear fit was used to obtain a theoretical DRCL spectrum of a mixture of 5% of Li_2O with 95% of V_2O_3. (b) Representation of the possible reaction mechanism of conversion or intercalation of two lithium into the V_2O_5 host lattice.

others, in situ/ex situ XRD, XANES, and Raman, clearly demonstrated that intercalation of lithium within α-V_2O_5 is largely associated with reversible structural modifications involving introduction of ions into a host structure, e.g. topochemical $\alpha \leftrightarrow \varepsilon \leftrightarrow \delta \leftrightarrow \gamma$ phase transformations for $Li_xV_2O_5$ ($0 < x < 2$).[23,3] However, surface sensitive techniques point to the possibility of Li_2O and V_2O_4 formation during the lithiation of α-V_2O_5. For example, the formation of a very thin, on the order of naometers, Li_2O layer at the surface of $Li_xV_2O_5$ nanowire was observed by in situ TEM/EELS.[14] Micro domains with Li-rich phases/concentration gradient were also observed by XANES/STXM at the lithiated $Li_xV_2O_5$ nanowire surface.[20] Nonetheless, uncertainties remain, as battery cathode materials system are known to be particularly sensitive to high keV beams. Phase transformation/lattice reconstruction induced by STEM/EELS experiments rather than a standard battery operation is frequently observed.[24] As the need for cathode materials with higher capacity and operating voltage, and hence with higher lithium content and lower structural stability, become greater, so does the need for nondestructive advanced diagnostics. Li_2MnO_3 is one of those promising cathode that exhibits heterogeneous phase transformation as well as band structure change as identified by Raman mapping and color variation of the delithiated thin film, respectively.[22]

In agreement with prior work,[14,23,48,3] using a nondestructive multimodal spectroscopies approach, this study reveals that electronic band structure and optical properties, as well as electrochemical performance, of V_2O_5-based cathode material are strongly influenced by how lithium ion deinsertion is done (cutoff voltage and number of cycles) and the associated phase transformation of the material. For example, the depth-resolved cathodoluminescence results reveal distinctive differences as a function of lithium intercalation/deintercalation and depth, suggesting severe changes in the vanadium environment. Surprisingly, when cycled multiple times, $Li_2V_2O_5$ exhibits features (Figure 5) that match almost perfectly the V_2O_3 ~2.5, ~3.1, and ~3.75 eV features, in particular at the surface.

However, these energies also coincide with two of the Li_2O peaks, at ~2.5 and ~3.1 eV (Figure 5). The formation of large amounts of V_2O_3 would involve a conversion reaction with the potential loss of oxygen (eq 1), which is of course irreversible.

$$Li_2V_2^{5+}O_5 \rightarrow Li_2O + V_2^{4+}O_4 \rightarrow Li_2O + V_2^{3+}O_3 + \frac{1}{2}O_{2(g)} \quad (1)$$

DRCLS results rule out this type of conversion of $Li_xV_2O_5$ into V_2O_3, V_2O_4, and Li_2O. Normalized CL spectra of Li_2O, V_2O_4, and V_2O_3 were compared with that of sample IV (see Figures 2, 3 and 4), as displayed in Figure 5, along with a model CL spectrum representing a 1-Li_2O to 19-V_2O_3 ratio mixture. With the intensity of Li_2O bands orders of magnitude stronger than any of the $Li_xV_2O_y$ spectra, it is apparent that the presence of even a small amount of Li_2O would vastly overshadow any other features, in particular the V_2O_3 peak at ~3.75 eV.

The electrochemical, optical response and, Raman results are consistent with this conclusion, further indicating that insertion is the dominant reaction mechanism, and precluding conversion reaction as a possibility. Indeed, despite hours of recording optical images during cycling, no bubbles were observed through the quartz windows of the electrochemical cell, which would have been indicative of oxygen gas evolution.

The relatively stable electrochemical capacity reinforces the hypothesis of an insertion process as opposed to a conversion reaction. Due to its irreversible nature, partial conversion is expected to induce severe capacity fading. However, a significant increase of the internal resistance is observed with cycling, along with major difference in the consistency of the color, especially at high voltage. The aforementioned electrochemical characteristics highlight the reversible nature of the insertion mechanism but suggests the possibility of the existence of multiple phases that blend at the macroscale while affecting lithium-ion transport. The Raman study supports the hypothesis of partial reversibility of the lithium insertion at deep discharge, where the long-range order is not restored. The coexistence of $\delta + \gamma$ or $\varepsilon + \alpha$ phases, which could be responsible for the lithium trapping effect, is inferred.

Thus, by combining the cathodoluminesence, electrochemistry, Raman and optical response, we conclude that lithiation/delithiation of V_2O_5 up to $Li_2V_2O_5$ is overwhelmingly an intercalation/deintercalation reaction rather than a conversion reaction. Contrary to prior experimental studies using hard X-ray spectroscopy based methods,[14,20] no formation of Li_2O was detected, even at the surface of the lithiated V_2O_5 thin films. However, our results imply that a nonfully uniform topochemical lithium insertion is occurring, with the coexistence of multiple metastable phases that blend

https://dx.doi.org/10.1021/acs.chemmater.0c01478
Chem. Mater. 2020, 32, 7226−7236

at the macroscale, below the ~1 μm spatial resolution of our Raman system.

In our previous work,[47] we extensively discussed the origin of the shift/disappearance of the ~1.8-2 eV peaks during the first lithiation from the DRCLS spectra and correlated it with crystallographic distortions of the V_2O_5's structure along its three axes. Further insight regarding the local atomic and electronic structure of the $Li_xV_2O_5$ phases can be deduced from the DRCLS results. In fact, a plausible alternative explanation for the CL spectra is centered around lithiation-induced alterations in local crystal structure of $Li_xV_2O_5$ and the accompanying modification of electronic and hence optical structure. The most critical question remains to determine the origin for the resemblance of the $Li_xV_2O_5$ features compared to that of V_2O_4 andV_2O_3.[49−51] Crystallographic representations of the aforementioned compounds are presented in Supporting Information (Figure S2 and S3). In V_2O_4 and V_2O_3, vanadium is in an octahedral environment of oxygen and the vanadium oxidation states are V^{4+} and V^{3+}, respectively. $V-O_{apical}$ bond distances are in the 1.8 to 2.1 Å range. The VO_5 compressed pyramid motif of α-V_2O_5 can be alternately described as a distorted VO_6 octahedral with a short (1.6 Å) and long (2.8 Å) out of plane V−O bond. As extensively described above, lithium insertion strongly affects the out of plane $V-O_{apical}$ bond properties and results in a reduction of vanadium from 5^+ to 4^+. It is conceivable that multiple Li deinsertions affect the electronic structure of $Li_xV_2O_5$ in such a way that the partial V_{3d} t_{2g} and O_{2p} density of states in the range we collected appear similar to those of V_2O_3 where vanadium is in the octahedral environment of oxygen (Figure S3c). Such a structure[52] is displayed in Figure 5 with six-coordinated vanadium in a layered type structure, allowing reversible lithium intercalation.

In addition, with extensive cycling, the relative intensity of the band at 4.2 eV compared to that of ~3.7 eV, increases with depth (Figure 4). This is also accompanied by a progressive shift of the feature at 3.7 eV toward higher energy. This effect could either originate from dangling bonds absorbed at the surface that generate a variation in local energy or changes in the V 3d e_g ($d_{x^2-y^2}$ and, d_{z^2}) components. As this effect is not observed after half a cycle but rather with extensive cycling, this decrease of the V t_{2g}/e_g ratio is possibly related to a structural reorganization associated with the presence of lithium leading to a reduction of the vanadium. The O_{apical}-Li bond formation, together with the strong Li^+-Li^+ repulsion, impedes oxygen movement along the *c* axis and impacts electron localization in the system. This electron delocalization affects the nonbonding t_{2g} band states observed as well as the V $3d_{x^2-y^2}$-O $2p_x/2p_y$ hybridization energy between 3.5 and 5 eV. For instance it has been suggested that the V 3d t_{2g} states can be filled by Li 2s electrons.[53] The formation of small polarons that would be expected to occupy the V 3d t_{2g}: d_{xy} lowest level[54] is a plausible explanation for the disappearance of the peak at 2 eV and relative increase of the V 3d e_g intensity at 4.2 eV with depth. This is also consistent with previous works[19,20] where DFT, STXM and XANES have been used to suggest that lithium insertion within V_2O_5 nanowires led to electron localization on low V $3d_{xy}$ orbitals, resulting in a reduction of the V $3d_{xy}$ feature intensity and subsequent V t_{2g}/eg ratio as well as a progressive shift of the t_{2g} feature at higher energies. Explanations involve lowest local symmetry/structural distortion with variation of the vanadyl bond together with lithium rich phase segregation. Further investigations are needed to explore these theories. This conclusion highlights the value of depth-dependent cathodoluminescence as a rich spectroscopy for interrogating the character of electrochemical reaction in battery materials.

CONCLUSIONS

In this work, we prepared well-characterized $Li_xV_2O_5$ thin films and evaluated their electrochemical performance as a function of lithiation level and cycling number. We developed and applied nondestructive in situ and ex situ spectroscopic methods and standard electrochemical techniques to relate the performance of $Li_xV_2O_5$ to phase transformations and the possible coexistence of multiple metastable phases. A direct comparison of the voltage range versus the capacity profiles over time demonstrated that a higher reversible capacity and higher lithium extraction is obtained by decreasing the lower cutoff voltage. Raman spectroscopy and optical spectroscopy experiments demonstrated that electrochemical intercalation of large amounts of lithium into V_2O_5 results in poorer electrochemical performance originating from the presence of multiple phases, pyramidal VO_5 distortion, and band structure changes. Depth-profiling cathodoluminescence studies confirmed that, at high lithium content and cycling number, significant irreversible structural rearrangements associated with partial electronic destabilization of the V−O framework are observed. This study offers unique insight into the impact of lithiation on the local variations of phase, electronic structure and, the associated mechanism of Li^+ transport in vanadium oxide-based Li-ion systems. Ultimately, we demonstrate that the combination of optical, Raman and cathodoluminescence response can be leveraged as a diagnostics platform for a wide variety of battery components. We directly measured $Li_xV_2O_5$ electronic and local atomic structure from the free surface to the thin film bulk several hundred nm below and its changes with respect to Li intercalation and cycling number on a near-nanometer scale with nondestructive tools. Cathodoluminescence is particularly sensitive to the presence of Li_2O, a common degradation phase in conversion cathodes. We deployed a new multimodal spectroscopy approach that permits us to differentiate between nonuniform topotactic and conversion reactions in electrochemically active ion-tunable transition metal oxide devices. Beyond this work, we plan to exploit this new platform and method to probe buried interfaces and formation of domain-conversion reaction in all-solid-state thin-film batteries to unveil the appropriate remedies to mitigate degradation processes, to guide further development of the battery system.

ASSOCIATED CONTENT

Supporting Information

The Supporting Information is available free of charge at https://pubs.acs.org/doi/10.1021/acs.chemmater.0c01478.

Further sample characterization: AFM images of $Li_xV_2O_5$ (x = 0−2) thin films; detailed information regarding crystallographic structure of $Li_xV_2O_5$ (x = 0−2), Li_2O, V_2O_4, and V_2O_3; table exhibiting battery performance metrics (PDF)

AUTHOR INFORMATION

Corresponding Author

Angelique Jarry − *Department of Materials Science and Engineering and Institute for Systems Research, University of*

https://dx.doi.org/10.1021/acs.chemmater.0c01478
Chem. Mater. 2020, 32, 7226−7236

Maryland, College Park, Maryland 20742, United States; orcid.org/0000-0002-5410-8020; Email: angeliquejarry@gmail.com

Authors

Mitchell Walker − *Department of Physics, The Ohio State University, Columbus, Ohio 43210, United States*

Stefan Theodoru − *Department of Materials Science and Engineering and Institute for Systems Research, University of Maryland, College Park, Maryland 20742, United States*

Leonard J. Brillson − *Department of Physics and Department of Electrical Engineering, The Ohio State University, Columbus, Ohio 43210, United States;* orcid.org/0000-0003-3527-9761

Gary W. Rubloff − *Department of Materials Science and Engineering and Institute for Systems Research, University of Maryland, College Park, Maryland 20742, United States*

Complete contact information is available at: https://pubs.acs.org/10.1021/acs.chemmater.0c01478

Author Contributions

A.J. developed the plans for the research with the assistance of G.W.R and L.B. A.J. prepared the V_2O_5 samples and carried out the electrochemical, optical, and Raman characterization with the help of S.T. M.W. carried out DRCLS characterization of the films. A.J. designed all of the figures and wrote the manuscript. All authors contributed and approved the final manuscript.

Notes

The authors declare no competing financial interest.

■ ACKNOWLEDGMENTS

This work was supported as part of the Nanostructures for Electrical Energy Storage (NEES), an Energy Frontier Research Center (EFRC) funded by the U.S. Department of Energy, Office of Science, Office of Basic Energy Sciences under Award Number DESC0001160 (A.J., S.T., and G.W.R.) and by the NSF Grant DMR-18-00130 (M.W. and L.B.). We also acknowledge the support of the Maryland Nanocenter.

■ REFERENCES

(1) Liu, C.; Neale, Z. G.; Cao, G. Understanding electrochemical potentials of cathode materials in rechargeable batteries. *Mater. Today* **2016**, *19*, 109−123.

(2) Mohanty, D.; Mazumder, B.; Devaraj, A.; Sefat, A. S.; Huq, A.; David, L. A.; Payzant, E. A.; Li, J.; Wood, D. L.; Daniel, C. Resolving the degradation pathways in high-voltage oxides for high-energy-density lithium-ion batteries; Alternation in chemistry, composition and crystal structures. *Nano Energy* **2017**, *36*, 76−84.

(3) Christensen, C. K.; Sørensen, D. R.; Hvam, J.; Ravnsbæk, D. B. Structural Evolution of Disordered $Li_xV_2O_5$ Bronzes in V_2O_5 Cathodes for Li-Ion Batteries. *Chem. Mater.* **2019**, *31*, 512−520.

(4) Manthiram, A.; Knight, J. C.; Myung, S. T.; Oh, S. M.; Sun, Y. K. Nickel-Rich and Lithium-Rich Layered Oxide Cathodes: Progress and Perspectives. *Adv. Energy Mater.* **2016**, *6*, 1501010.

(5) Seo, D.-H.; Lee, J.; Urban, A.; Malik, R.; Kang, S.; Ceder, G. The structural and chemical origin of the oxygen redox activity in layered and cation-disordered Li-excess cathode materials. *Nat. Chem.* **2016**, *8*, 692.

(6) Delmas, C. Operating through oxygen. *Nat. Chem.* **2016**, *8*, 641.

(7) Richards, W. D.; Dacek, S. T.; Kitchaev, D. A.; Ceder, G. Fluorination of Lithium-Excess Transition Metal Oxide Cathode Materials. *Adv. Energy Mater.* **2018**, *8*, 1701533.

(8) Urban, A.; Lee, J.; Ceder, G. The Configurational Space of Rocksalt-Type Oxides for High-Capacity Lithium Battery Electrodes. *Adv. Energy Mater.* **2014**, *4*, 1400478.

(9) Xu, B.; Fell, C. R.; Chi, M.; Meng, Y. S. Identifying surface structural changes in layered Li-excess nickel manganese oxides in high voltage lithium ion batteries: A joint experimental and theoretical study. *Energy Environ. Sci.* **2011**, *4*, 2223−2233.

(10) Galy, J. Vanadium pentoxide and vanadium oxide bronzes—Structural chemistry of single (S) and double (D) layer $M_xV_2O_5$ phases. *J. Solid State Chem.* **1992**, *100*, 229−245.

(11) Mukherjee, A.; Sa, N.; Phillips, P. J.; Burrell, A.; Vaughey, J.; Klie, R. F. Direct Investigation of Mg Intercalation into the Orthorhombic V_2O_5 Cathode Using Atomic-Resolution Transmission Electron Microscopy. *Chem. Mater.* **2017**, *29*, 2218−2226.

(12) Delmas, C.; Brèthes, S.; Ménétrier, M. ω-$Li_xV_2O_5$ — a new electrode material for rechargeable lithium batteries. *J. Power Sources* **1991**, *34*, 113−118.

(13) Lin, F.; Markus, I. M.; Nordlund, D.; Weng, T.-C.; Asta, M. D.; Xin, H. L.; Doeff, M. M. Surface reconstruction and chemical evolution of stoichiometric layered cathode materials for lithium-ion batteries. *Nat. Commun.* **2014**, *5*, 3529.

(14) Mukherjee, A.; Ardakani, H. A.; Yi, T.; Cabana, J.; Shahbazian-Yassar, R.; Klie, R. F. Direct characterization of the Li intercalation mechanism into α-V_2O_5 nanowires using in-situ transmission electron microscopy. *Appl. Phys. Lett.* **2017**, *110*, 213903.

(15) Yu, Y.; Li, J.; Wang, X.; Chang, B.; Wang, J.; Ahmad, M.; Sun, H. Oxygen vacancies enhance lithium storage performance in ultralong vanadium pentoxide nanobelt cathodes. *J. Colloid Interface Sci.* **2019**, *539*, 118−125.

(16) Gao, X.; Ikuhara, Y. H.; Fisher, C. A. J.; Huang, R.; Kuwabara, A.; Moriwake, H.; Kohama, K.; Ikuhara, Y. Oxygen loss and surface degradation during electrochemical cycling of lithium-ion battery cathode material $LiMn_2O_4$. *J. Mater. Chem. A* **2019**, *7*, 8845−8854.

(17) Qian, D.; Xu, B.; Chi, M.; Meng, Y. S. Uncovering the roles of oxygen vacancies in cation migration in lithium excess layered oxides. *Phys. Chem. Chem. Phys.* **2014**, *16*, 14665−14668.

(18) Jarry, A.; Gottis, S.; Yu, Y.-S.; Roque-Rosell, J.; Kim, C.; Cabana, J.; Kerr, J.; Kostecki, R. The Formation Mechanism of Fluorescent Metal Complexes at the $Li_xNi_{0.5}Mn_{1.5}O_{4-\delta}$/Carbonate Ester Electrolyte Interface. *J. Am. Chem. Soc.* **2015**, *137*, 3533−3539.

(19) De Jesus, L. R.; Horrocks, G. A.; Liang, Y.; Parija, A.; Jaye, C.; Wangoh, L.; Wang, J.; Fischer, D. A.; Piper, L. F. J.; Prendergast, D.; Banerjee, S. Mapping polaronic states and lithiation gradients in individual V_2O_5 nanowires. *Nat. Commun.* **2016**, *7*, 12022.

(20) Horrocks, G. A.; Braham, E. J.; Liang, Y.; De Jesus, L. R.; Jude, J.; Velázquez, J. M.; Prendergast, D.; Banerjee, S. Vanadium K-Edge X-ray Absorption Spectroscopy as a Probe of the Heterogeneous Lithiation of V_2O_5: First-Principles Modeling and Principal Component Analysis. *J. Phys. Chem. C* **2016**, *120*, 23922−23932.

(21) Strelcov, E.; Cothren, J.; Leonard, D.; Borisevich, A. Y.; Kolmakov, A. In situ SEM study of lithium intercalation in individual V_2O_5 nanowires. *Nanoscale* **2015**, *7*, 3022−3027.

(22) Ruther, R. E.; Dixit, H.; Pezeshki, A. M.; Sacci, R. L.; Cooper, V. R.; Nanda, J.; Veith, G. M. Correlating Local Structure with Electrochemical Activity in Li_2MnO_3. *J. Phys. Chem. C* **2015**, *119*, 18022−18029.

(23) Huo, D.; Contreras, A.; Laïk, B.; Bonnet, P.; Guérin, K.; Muller-Bouvet, D.; Cenac-Morthe, C.; Baddour-Hadjean, R.; Pereira-Ramos, J. P. Evidence for a nanosize effect on the structural and high performance electrochemical properties of V_2O_5 obtained via fluorine chemistry. *Electrochim. Acta* **2017**, *245*, 350−360.

(24) Lin, F.; Markus, I. M.; Doeff, M. M.; Xin, H. L. Chemical and Structural Stability of Lithium-Ion Battery Electrode Materials under Electron Beam. *Sci. Rep.* **2015**, *4*, 5694.

(25) Zhang, C.; Yang, Q.; Koughia, C.; Ye, F.; Sanayei, M.; Wen, S.-J.; Kasap, S. Characterization of vanadium oxide thin films with different stoichiometry using Raman spectroscopy. *Thin Solid Films* **2016**, *620*, 64−69.

(26) Chen, X.; Pomerantseva, E.; Banerjee, P.; Gregorczyk, K.; Ghodssi, R.; Rubloff, G. Ozone-Based Atomic Layer Deposition of Crystalline V_2O_5 Films for High Performance Electrochemical Energy Storage. *Chem. Mater.* **2012**, *24*, 1255−1261.
(27) Baddour-Hadjean, R.; Pereira-Ramos, J. P.; Navone, C.; Smirnov, M. Raman Microspectrometry Study of Electrochemical Lithium Intercalation into Sputtered Crystalline V_2O_5 Thin Films. *Chem. Mater.* **2008**, *20*, 1916−1923.
(28) Muñoz-Castro, M.; Berkemeier, F.; Schmitz, G.; Buchheit, A.; Wiemhöfer, H.-D. Controlling the optical properties of sputtered-deposited $Li_xV_2O_5$ films. *J. Appl. Phys.* **2016**, *120*, 135106.
(29) Wang, Q.; Brier, M.; Joshi, S.; Puntambekar, A.; Chakrapani, V. Defect-induced Burstein-Moss shift in reduced V_2O_5 nanostructures. *Phys. Rev. B: Condens. Matter Mater. Phys.* **2016**, *94*, 245305.
(30) Mjejri, I.; Manceriu, L. M.; Gaudon, M.; Rougier, A.; Sediri, F. Nano-vanadium pentoxide films for electrochromic displays. *Solid State Ionics* **2016**, *292*, 8−14.
(31) Zimmermann, R.; Claessen, R.; Reinert, F.; Steiner, P.; Hüfner, S. Strong hybridization in vanadium oxides: evidence from photo-emission and absorption spectroscopy. *J. Phys.: Condens. Matter* **1998**, *10*, 5697−5716.
(32) Eyert, V.; Höck, K. H. Electronic structure of V_2O_5: Role of octahedral deformations. *Phys. Rev. B: Condens. Matter Mater. Phys.* **1998**, *57*, 12727−12737.
(33) Drouin, D.; Couture, A. R.; Joly, D.; Tastet, X.; Aimez, V.; Gauvin, R. CASINO V2.42—A Fast and Easy-to-use Modeling Tool for Scanning Electron Microscopy and Microanalysis Users. *Scanning* **2007**, *29*, 92−101.
(34) Hovington, P.; Drouin, D.; Gauvin, R. CASINO: A new monte carlo code in C language for electron beam interaction —part I: Description of the program. *Scanning* **1997**, *19*, 1−14.
(35) Schweiger, H.-G.; Obeidi, O.; Komesker, O.; Raschke, A.; Schiemann, M.; Zehner, C.; Gehnen, M.; Keller, M.; Birke, P. Comparison of Several Methods for Determining the Internal Resistance of Lithium Ion Cells. *Sensors* **2010**, *10*, 5604−5625.
(36) Delmas, C.; Cognac-Auradou, H.; Cocciantelli, J. M.; Ménétrier, M.; Doumerc, J. P. The $Li_xV_2O_5$ system: An overview of the structure modifications induced by the lithium intercalation. *Solid State Ionics* **1994**, *69*, 257−264.
(37) Jain, R. K.; Khanna, A. Structural, optical and electrical properties of crystalline V_2O_5 films deposited by thermal evaporation and effects of temperature on UV−vis and Raman spectra. *Optik* **2017**, *144*, 271−280.
(38) Baddour-Hadjean, R.; Pereira-Ramos, J.-P. Raman Microspectrometry Applied to the Study of Electrode Materials for Lithium Batteries. *Chem. Rev.* **2010**, *110*, 1278−1319.
(39) Jung, H.; Gerasopoulos, K.; Talin, A. A.; Ghodssi, R. A platform for in situ Raman and stress characterizations of V_2O_5 cathode using MEMS device. *Electrochim. Acta* **2017**, *242*, 227−239.
(40) Ramana, C. V.; Smith, R. J.; Hussain, O. M.; Massot, M.; Julien, C. M. Surface analysis of pulsed laser-deposited V_2O_5 thin films and their lithium intercalated products studied by Raman spectroscopy. *Surf. Interface Anal.* **2005**, *37*, 406−411.
(41) Baddour-Hadjean, R.; Golabkan, V.; Pereira-Ramos, J. P.; Mantoux, A.; Lincot, D. A Raman study of the lithium insertion process in vanadium pentoxide thin films deposited by atomic layer deposition. *J. Raman Spectrosc.* **2002**, *33*, 631−638.
(42) Kerlau, M.; Marcinek, M.; Srinivasan, V.; Kostecki, R. M. Studies of local degradation phenomena in composite cathodes for lithium-ion batteries. *Electrochim. Acta* **2007**, *52*, 5422−5429.
(43) Kumar, S.; Maury, F.; Bahlawane, N. Electrical Switching in Semiconductor-Metal Self-Assembled VO_2 Disordered Metamaterial Coatings. *Sci. Rep.* **2016**, *6*, 37699.
(44) Coenen, T.; Haegel, N. M. Cathodoluminescence for the 21st century: Learning more from light. *Appl. Phys. Rev.* **2017**, *4*, 031103.
(45) Brillson, L. J. Applications of depth-resolved cathodoluminescence spectroscopy. *J. Phys. D: Appl. Phys.* **2012**, *45*, 183001.
(46) Díaz-Guerra, C.; Piqueras, J. Thermal Deposition Growth and Luminescence Properties of Single-Crystalline V_2O_5 Elongated Nanostructures. *Cryst. Growth Des.* **2008**, *8*, 1031−1034.
(47) Walker, M. J.; Jarry, A.; Pronin, N.; Ballard, J.; Rubloff, G. W.; Brillson, L. J. Nanoscale depth and lithiation dependence of V_2O_5 band structure by cathodoluminescence spectroscopy. *J. Mater. Chem. A* **2020**, *8*, 11800−11810.
(48) Rao, K. J.; Pecquenard, B.; Gies, A.; Levasseur, A.; Etourneau, J. Structural and electrochemical behaviour of sputtered vanadium oxide films: oxygen non-stoichiometry and lithium ion sequestration. *Bull. Mater. Sci.* **2006**, *29*, 535−546.
(49) Bhuyan, P. D.; Gupta, S. K.; Kumar, A.; Sonvane, Y.; Gajjar, P. N. Highly infrared sensitive VO_2 nanowires for a nano-optical device. *Phys. Chem. Chem. Phys.* **2018**, *20*, 11109−11115.
(50) Peter, A. P.; Martens, K.; Rampelberg, G.; Toeller, M.; Ablett, J. M.; Meersschaut, J.; Cuypers, D.; Franquet, A.; Detavernier, C.; Rueff, J.-P.; Schaekers, M.; Van Elshocht, S.; Jurczak, M.; Adelmann, C.; Radu, I. P. Metal-Insulator Transition in ALD VO_2 Ultrathin Films and Nanoparticles: Morphological Control. *Adv. Funct. Mater.* **2015**, *25*, 679−686.
(51) Kim, H.-T.; Chae, B.-G.; Youn, D.-H.; Maeng, S.-L.; Kim, G.; Kang, K.-Y.; Lim, Y.-S. Mechanism and observation of Mott transition in VO_2-based two- and three-terminal devices. *New J. Phys.* **2004**, *6*, 52−52.
(52) Jain, A.; Ong, S. P.; Hautier, G.; Chen, W.; Richards, W. D.; Dacek, S.; Cholia, S.; Gunter, D.; Skinner, D.; Ceder, G.; Persson, K. A. Commentary: The Materials Project: A materials genome approach to accelerating materials innovation. *APL Mater.* **2013**, *1*, 011002.
(53) Smirnov, M. B.; Roginskii, E. M.; Kazimirov, V. Y.; Smirnov, K. S.; Baddour-Hadjean, R.; Pereira-Ramos, J. P.; Zhandun, V. S. Spectroscopic and Computational Study of Structural Changes in γ-LiV_2O_5 Cathodic Material Induced by Lithium Intercalation. *J. Phys. Chem. C* **2015**, *119*, 20801−20809.
(54) Watthaisong, P.; Jungthawan, S.; Hirunsit, P.; Suthirakun, S. Transport properties of electron small polarons in a V_2O_5 cathode of Li-ion batteries: a computational study. *RSC Adv.* **2019**, *9*, 19483−19494.

https://dx.doi.org/10.1021/acs.chemmater.0c01478
Chem. Mater. 2020, 32, 7226−7236

Supplementary information: Elucidating Structural Transformations in $Li_xV_2O_5$ Electrochromic Thin Films by Multimodal Spectroscopies

Angelique Jarry*[1], Mitchell Walker[2], Stefan Theodoru[1], Leonard J. Brillson[2,3], and Gary W. Rubloff[1]

[1]Department of Materials Science and Engineering, University of Maryland, College Park, MD 20742

[2]Department of Physics, The Ohio State University, Columbus, OH 43210 USA

[3]Department of Electrical Engineering, The Ohio State University, Columbus, OH 43210 USA

Corresponding author: angeliquejarry@gmail.com

Surface roughness of $Li_xV_2O_5$ as a function of lithiation.

Surface roughness as determined by atomic force microscopy is displayed in Figure 1. In agreement with the Raman response, the lithiation leads to a progressive amorphization of the phase.

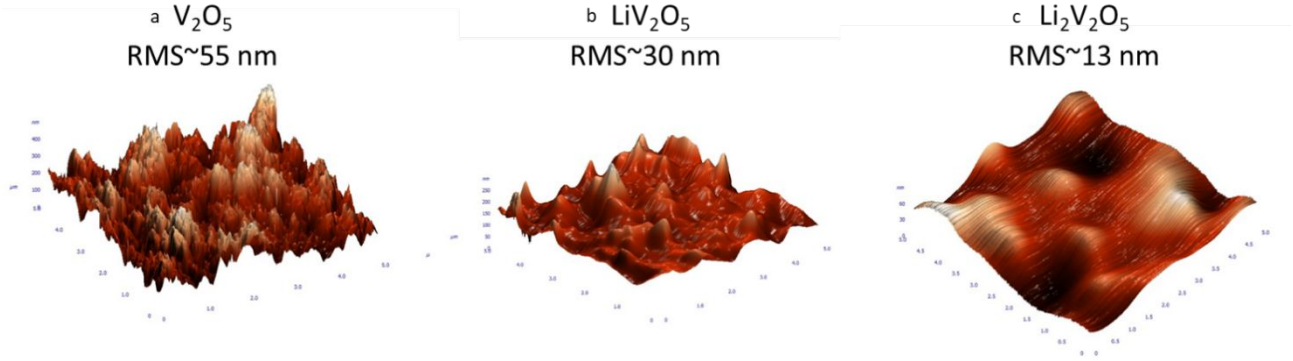

Figure 1: Atomic force microscopy 3D images of $Li_xV_2O_5$ (x = 0 ; 1 ; 2) and associated roughness. Images are 5 microns by 5 microns with heights z in nm.

Crystal structure and associated electrochemistry of $Li_xV_2O_5$ polymorphs.

The effect of electrochemical intercalation of lithium on the vanadium oxides' crystallographic structures have been extensively studied since the seventies.[1] As depicted in Figure 2, the evolution of the long-range structure of $Li_xV_2O_5$ ($0 < x < 2$) during the lithium insertion process is generally accepted to occur via the following sequence $\gamma \rightarrow \delta \rightarrow \varepsilon \rightarrow \alpha$.[1, 2] The α layered structure consists of infinite layers of alternating pairs of VO_5 pyramids connected by the edges and corners bound by van der Waals interactions. $\gamma \rightarrow \delta \rightarrow \varepsilon \rightarrow \alpha$ phase transformations involve

substantial puckering, rotation and gliding of the VO_5 pyramids as well as an increase in interlayer spacing. However, these transitions are considered topotactic, i.e reversible structural modifications involving introduction of ions into a host structure, with a symmetry that remains orthorhombic (ε ; α: P mmn $\delta \rightarrow$: A mam $\gamma \rightarrow$: P nma). Hence, the transformation is fully reversible at low x ($x \leq 1$) and mostly reversible for higher value ($1 \leq x \leq 2$). To accommodate more than two lithium per unit cell, the system has to undergo a non-reversible phase transformation to a cubic rock salt structure where vanadium and lithium are randomly distributed within the same atomic crystallographic site,[3] leading to a drastic decrease of the electrochemical performance. As this study focuses on diagnostics of standard battery operation degradation mechanisms rather than the total loss of structural integrity, intercalation involving more than two lithium will not be discussed further herein. Instead we will center our attention on the topochemical $\gamma \leftrightarrow \delta \leftrightarrow \varepsilon \leftrightarrow \alpha$ phase transformations with $Li_xV_2O_5$ ($0 < x < 2$) for a maximal theoretical capacity of 285 mAh/g.

Figure 2 shows the first galvanostatic charge of the $Li_xV_2O_5$ ($0 < x < 2$) thin film up to 2.2V at a ~C/25 rate, i.e., 25 hours for a charge. From high to low voltage, a first plateau is observed at 3.2V that corresponds to the formation of ε-$Li_xV_2O_5$, followed by a sharp potential drop near 3.1V up to 2.3V for δ-$Li_xV_2O_5$. The following lower voltage step is related to γ-$Li_xV_2O_5$ with $1 < x < 2$. As seen in Figure 2, the amount of lithium inserted into the structure is directly correlated to the cut-off voltage applied during the electrochemical cycling of the $Li_xV_2O_5$ thin films.[1, 2] 2.2 V vs. Li/Li^+ is just below the second voltage plateau at 2.3V where the γ phase is expected to be formed. Hence, by fine-tuning the current applied, that governs the rate of lithium intercalation to match as closely as possible the chemical reaction kinetics, one will expect the homogeneous de-intercalation of approximately two lithium within the structure, to obtain a single-phase γ-$Li_2V_2O_5$ at 2.2V.[1] To support the discussion in the manuscript related to the possibility of a conversion reaction, the room temperature structure of Li_2O, V_2O_4 and V_2O_3 are displayed in Figure 3.

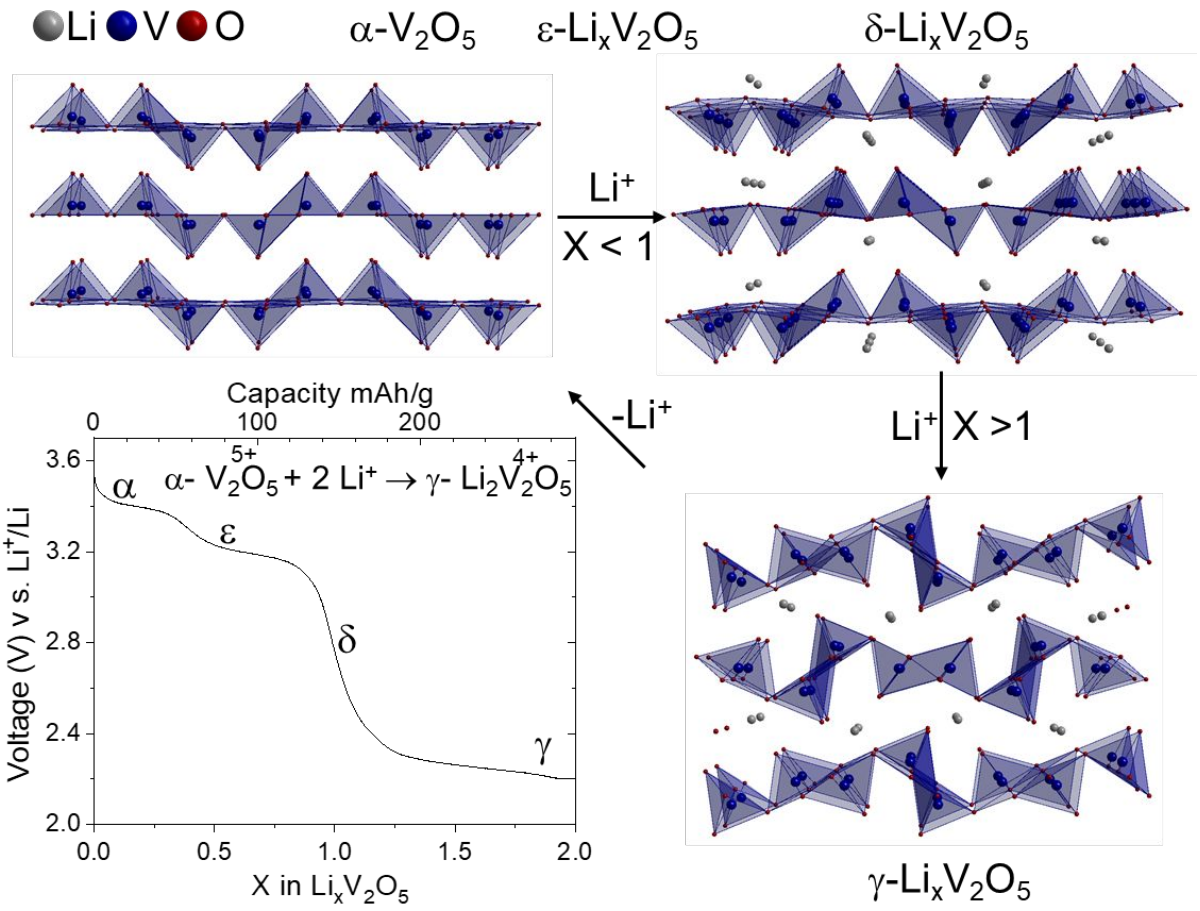

Figure 2: Representation of the crystallographic structure evolution of $Li_xV_2O_5$ as a function of the lithiation level as dictated by the electrochemistry

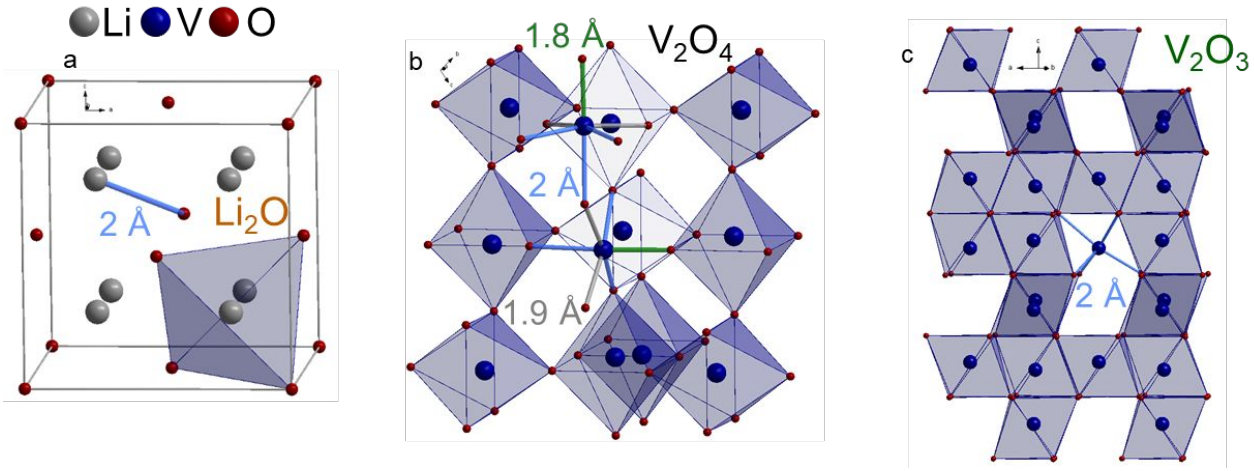

Figure 3: Representation of the crystallographic structure of Li_2O, V_2O_4 and V_2O_3 at room temperature.

Battery performance.

Table 2: Battery performance metrics (delivered capacity, internal resistance, and polarization) as a function of voltage range and cycling number.

Voltage range (V)	3.4-2.2 for two li^+ insertion		3.4-2.8 for one li^+ insertion	
Cycle number	0.5-1	5.5-6	0.5-1	5.5-6
Capacity delivered (mAh/g)	262	255	145	133
Polarization high cut-off voltage (ΔmV/hrs)	3	26	80	45
Polarization low cut-off voltage (ΔmV/hrs)	20	80	111	96
Internal Resistance high cut-off voltage (Ω)	350	2175	5500	4000
Internal Resistance low cut-off voltage (Ω)	1750	5000	12000	8950

Acknowledgments

This work was supported as part of the Nanostructures for Electrical Energy Storage (NEES), an Energy Frontier Research Center (EFRC) funded by the U.S. Department of Energy, Office of Science, Office of Basic Energy Sciences under Award Number DESC0001160 (A.J., S.T. and G.W.R.) and by the NSF grant DMR-18-00130 (M.W. and L.B.). We also acknowledge the support of the Maryland Nanocenter.

References

(1) Delmas, C.; Cognac-Auradou, H.; Cocciantelli, J. M.; Ménétrier, M.; Doumerc, J. P., The $Li_xV_2O_5$ system: An overview of the structure modifications induced by the lithium intercalation. *Solid State Ionics,* **1994,** *69*, 257-264.

(2) Baddour-Hadjean, R.; Safrany Renard, M.; Pereira-Ramos, J. P., Unraveling the structural mechanism of Li insertion in γ'-V_2O_5 and its effect on cycling properties. *Acta Materialia,* **2019,** *165*, 183-191.

(3) Christensen, C. K.; Sørensen, D. R.; Hvam, J.; Ravnsbæk, D. B., Structural Evolution of Disordered $Li_xV_2O_5$ Bronzes in V_2O_5 Cathodes for Li-Ion Batteries. *Chemistry of Materials,* **2019,** *31*, 512-520.